ORIGINAL ARTICLE

INTEGRATED HYDROLOGICAL-HYDRAULIC MODELING FOR FLASH-FLOOD INUNDATION EXPOSURE ASSESSMENT

Ficky Marcellino Oroh[1*], Cindy Jeane Supit[1*], Tommy Miran[2*]
[1] Universitas Sam Ratulangi, Manado, Indonesia
[2] Balai Wilayah Sungai Sulawesi I, Manado, Indonesia
*Corresponding Author: fickyoroh19@unsrat.ac.id

ABSTRACT

Flash floods in small tropical catchments require spatially explicit analysis, yet data scarcity often limits model verification. This study integrates HEC-HMS rainfall-runoff modeling and HEC-RAS two-dimensional hydraulic simulation to reconstruct the 19 February 2017 flood in the Nuay River watershed and to assess village-scale inundation exposure. Annual-maximum daily rainfall records for 2014-2024 were compiled from the Ranowangko Tara-Tara and Tondano-Paleloan stations. Missing Tondano-Paleloan observations in 2015, 2021, and 2024 were not treated as zero; Thiessen weights were renormalized to the available station for those years. The corrected annual-maximum series was analyzed with the Log Pearson Type III distribution, giving design rainfall from 111.39 mm for the 2-year return period to 283.57 mm for the 1,000-year return period. The reconstructed 2017 HEC-HMS event produced a peak discharge of 20.0 m3/s at 03:00. HEC-RAS 2D outputs show inundation concentrated near the river corridor and low-lying terrain, with displayed depth classes extending from less than 1 m to 5 m. Talikuran Satu and Tounelet Satu had the largest inundated-area proportions, 3.2% and 2.1%, respectively. These classes are interpreted as inundation exposure rather than comprehensive flood risk because population, assets, vulnerability, and velocity were not included. The integrated workflow supports screening-level mitigation prioritization, while uncertainty remains due to the short rainfall record, event-based non-gauged calibration evidence, and incomplete hydraulic-project metadata.

Keywords: flash flood, flood hazard, HEC-HMS, HEC-RAS 2D, inundation exposure

INTRODUCTION

Floods are among the most recurrent hydrometeorological hazards and can produce major losses to people, infrastructure, agricultural production, and local economies. The severity of flash flooding is amplified in small catchments because rainfall can be converted into concentrated runoff over short response times, leaving limited opportunity for warning and emergency action. Contemporary flood assessment therefore increasingly combines rainfall-runoff simulation with hydraulic or hydrodynamic modeling so that hydrographs generated at catchment scale can be translated into spatially explicit depth and inundation patterns (Peker et al., 2024; El-Bagoury & Gad, 2024; Mkhonta et al., 2026). Recent event-reconstruction studies further show that integrated hydrological-hydraulic approaches are particularly valuable where post-event evidence must compensate for sparse streamflow monitoring (Xu et al., 2025).

Flood-inundation modeling has evolved from one-dimensional channel representations toward two-dimensional approaches that better represent lateral flow paths, floodplain storage, flow redistribution, and local topographic controls. Foundational comparisons showed that the added spatial freedom of two-dimensional models can improve the representation of complex inundation processes, although model performance remains sensitive to the quality of terrain, boundary conditions, grid or mesh resolution, and roughness parameterization (Horritt & Bates, 2002; Horritt et al., 2006; Hunter et al., 2007). Efficient shallow-water formulations and subgrid approaches have subsequently expanded the practical scale of two-dimensional modeling (Bates et al., 2010; Neal et al., 2012). HEC-RAS 2D is now widely used within this family of tools and has shown useful performance in comparative and application studies involving complex topography and flash-flood settings (Shustikova et al., 2019; Jeong et al., 2024).

The scientific value of inundation maps depends on more than the hydraulic solver. High-resolution model studies demonstrate that flood extent and depth can change materially with topographic representation, computational scale, and surface roughness (Fewtrell et al., 2011; Liu et al., 2019).

Systematic uncertainty analysis also shows that hydrologic inflow uncertainty, friction parameters, numerical structure, and representation of built or channel features may all propagate into mapped outcomes (Willis et al., 2019). Consequently, maps should be interpreted as model-based estimates conditioned by data and parameter assumptions rather than as deterministic boundaries. This consideration is especially important for small data-scarce basins, where local observations may be sufficient for event consistency checks but insufficient for formal calibration and independent validation.

A second conceptual issue concerns the distinction between flood hazard, exposure, and risk. Flood hazard describes the physical characteristics and probability of potentially damaging flooding, while exposure identifies people, assets, or areas located within the hazard footprint; risk additionally depends on vulnerability and potential consequences. Flood-risk frameworks therefore combine multiple dimensions instead of relying on inundated area alone (de Moel et al., 2009; Merz et al., 2010; Koks et al., 2015). Studies of risk-analysis detail and flash-flood assessment have similarly shown that a physically plausible inundation footprint is necessary but not sufficient for a comprehensive risk estimate (Apel et al., 2009; Li et al., 2019). For this reason, the present revision uses the term inundation exposure for village classifications based on the percentage of administrative area inundated and does not equate that percentage with full socioeconomic flood risk.

At broader scales, advances in continental and global hazard mapping demonstrate the utility of physically informed inundation modeling for comparative planning, but they also underline the need for local validation when maps are used for site-specific decisions (Alfieri et al., 2014; Dottori et al., 2016; Sampson et al., 2015; Wing et al., 2017). Reviews of flood-hazard mapping methods and urban flood simulation reinforce this point: model selection should follow the intended decision scale, available observations, and uncertainty that can be justified (Mudashiru et al., 2021; Luo et al., 2022; Teng et al., 2017). Accordingly, a small-catchment application should make the quantitative chain from rainfall data to hydrograph and inundation extent traceable, while avoiding unsupported precision.

The Nuay River is located in Sonder District, Minahasa Regency, North Sulawesi, and supports local water-resource and agricultural functions. A recent water-balance study at the Nuay diversion weir confirms the hydrological importance of the catchment for irrigation and local water management (Wilar et al., 2024). However, existing regional work has mainly addressed river capacity, design floods, rainfall temporal distribution, or water availability rather than an integrated event-based rainfall-runoff and two-dimensional inundation reconstruction. For example, Montolalu et al. (2021) evaluated cross-sectional capacity for planned flooding in the nearby Sonder area, while Salem et al. (2016) examined hourly rainfall distribution patterns around Manado. These studies provide important regional context but do not resolve how a rapid catchment response is translated into spatial flood exposure along the Nuay River.

The research gap is therefore both empirical and methodological. Empirically, spatially explicit flash-flood information for the Nuay River corridor is limited. Methodologically, the available local evidence has not been organized into a transparent chain that (i) handles incomplete rainfall records without treating missing observations as zero, (ii) reports the statistical basis of design-rainfall selection, (iii) distinguishes reconstructed-event output from return-period analysis, and (iv) separates inundation exposure from comprehensive risk. The novelty of this study lies not in introducing a new hydrological or hydraulic algorithm, but in applying an auditable integrated workflow to a small tropical, data-scarce catchment and explicitly documenting the limits of inference. The study therefore aims to reconstruct the 19 February 2017 flood using HEC-HMS and HEC-RAS 2D, quantify the corrected rainfall-frequency characteristics, map flood depth and inundation extent, classify village-scale inundation exposure using transparent thresholds, and identify the implications and uncertainties relevant to local mitigation planning.

METHOD

This study used a quantitative event-reconstruction design that links hydrological frequency analysis, rainfall-runoff modeling, two-dimensional hydraulic simulation, and GIS-based spatial interpretation. The analytical sequence was designed to preserve traceability between observed rainfall information, HEC-HMS discharge generation, HEC-RAS 2D inundation output, and village-scale exposure statistics.

The workflow follows the broad coupled-modeling logic used in recent HEC-HMS/HEC-RAS applications while reporting data limitations explicitly rather than substituting unverified parameter details (Peker et al., 2024; El-Bagoury & Gad, 2024; Mkhonta et al., 2026).

Study Area

The study area is the Nuay River watershed in and around Tounelet Village, Sonder District, Minahasa Regency, North Sulawesi Province. The catchment is small and drains a landscape composed primarily of agricultural and residential land with variable terrain and several relatively narrow river sections. These characteristics are relevant to flash-flood behavior because short travel distances can produce a rapid hydrograph, while constricted or low-gradient channel sections can promote overbank flow. The study subject is the coupled hydrological-hydraulic response of the watershed, including rainfall characteristics, runoff generation, river geometry, water-surface behavior, inundation depth, and spatial inundation extent. Figure 1 locates the modeled river corridor and the discharge-measurement area used in the original study record.

Figure 1. Study-area location and Nuay River alignment used for field and model setup

Data Sources, Completeness, and Research Instruments

The analysis used secondary maximum-daily rainfall data from the MRG Ranowangko Tara-Tara station and the Tondano-Paleloan climatological station for 2014-2024, together with watershed, land-use, topographic, and GIS layers. Primary information consisted of field measurements of river cross-sections used to represent channel geometry. The original manuscript identifies the Sulawesi River Basin Organization I as the source of the rainfall record. The available project materials include field geometry figures and model-output screenshots but do not preserve every raw spatial layer or model project file. This revision therefore distinguishes directly documented inputs from parameters that cannot be independently recovered.

Table 1. Maximum Daily Rainfall Record Used in the Analysis

Year	Ranowangko Tara-Tara (mm)	Tondano-Paleloan (mm)
2014	196.5	110.50
2015	112.4	Missing
2016	102.0	115.50
2017	92.0	160.20

Year	Ranowangko Tara-Tara (mm)	Tondano-Paleloan (mm)
2018	105.5	126.50
2019	68.5	157.30
2020	107.0	157.30
2021	135.5	Missing
2022	124.0	99.80
2023	124.0	118.40
2024	109.0	Missing

Source: Sulawesi River Basin Organization I, as reported in the supplied manuscript. "Missing" indicates no value was available in the supplied record.

Three Tondano-Paleloan values are missing: 2015, 2021, and 2024. In the earlier areal-rainfall table, the weighted averages for those years were lower than the available Ranowangko values, which is consistent with inadvertently retaining the missing station weight without a valid observation. To remove that bias, this revision does not assign zero to a missing station. The Thiessen influence areas of 14.78 km2 and 1.22 km2 (total 16.00 km2) are retained when both stations are present; when Tondano-Paleloan is missing, the weight of the available Ranowangko observation is renormalized to 1.00 for that year. This treatment preserves the observed annual maximum rather than imposing an artificial rainfall deficit. It does not constitute statistical gap-filling and therefore avoids manufacturing an unobserved station value.

Research instruments comprised the rainfall and spatial datasets, field surveying equipment for river geometry, GIS/Global Mapper tools, HEC-HMS for rainfall-runoff simulation, and HEC-RAS 2D for unsteady hydraulic simulation. The exact software version numbers were not included in the supplied manuscript or screenshots in a form that could be verified; consequently, no version number is invented in this revision. This missing metadata is reported as a reproducibility limitation.

Hydrological Analysis

Areal rainfall was computed using Thiessen area weights. For years with two valid observations, the watershed rainfall was calculated as the sum of each station rainfall multiplied by its proportional influence area. For years with one missing station, the remaining valid weight was renormalized so that the active weights summed to one. Annual-maximum watershed rainfall was then used for frequency analysis. Descriptive statistics included the arithmetic mean, sample standard deviation, coefficient of variation, skewness, and kurtosis. The Log Pearson Type III (LP3) model was fitted to base-10 logarithms of the corrected annual-maximum series. Because only 11 annual maxima were available, the goodness-of-fit assessment is treated as an indicative diagnostic rather than definitive proof of distributional adequacy.

Effective rainfall in the HEC-HMS loss method was represented with the Soil Conservation Service Curve Number formulation. The equations are stated explicitly to make the hydrological procedure reproducible:

$$Pe = (P - 0.2S)^2 / (P + 0.8S), \text{ for } P > 0.2S; \text{ otherwise } Pe = 0. \quad (1)$$

$$S = 25400 / CN - 254 \quad (2)$$

where Pe is effective rainfall depth (mm), P is total rainfall depth (mm), S is maximum potential retention (mm), and CN is the dimensionless Curve Number. Rainfall excess was transformed to runoff with the SCS Synthetic Unit Hydrograph, and baseflow was represented by the recession method. The calibrated composite CN retained in the supplied model summary is 64. The project package does not contain the original land-use/soil lookup table used to derive or initialize this composite value, so the

CN should be interpreted as the retained event-model parameter rather than as an independently reproducible land-cover statistic.

Event Calibration and Reconstruction

The original study calibrated the HEC-HMS model using community-observed flood-stage information for the 19 February 2017 event and described a conversion of observed stage to discharge through regional analysis. However, the supplied revision materials do not include a continuous observed discharge hydrograph, the observation time series, a site-specific rating curve, or the regionalization equation. Accordingly, the present revision treats the community-reported information as an event-consistency constraint rather than claiming a statistically verified discharge calibration. Standard hydrological performance statistics such as Nash-Sutcliffe efficiency, Kling-Gupta efficiency, RMSE, or percent bias require temporally paired observed and simulated discharge series (Nash & Sutcliffe, 1970; Gupta et al., 2009; Moriasi et al., 2007); those series are unavailable in the supplied record, and therefore these statistics are not fabricated. No independent validation event was available in the supplied materials.

The retained event parameters are Curve Number 64, recession constant 0.4, ratio to peak 0.6, initial discharge 0.142813 m3/s, and lag time 60 minutes. Figure 2 summarizes the original workflow from field survey and data collection through HEC-HMS and HEC-RAS 2D simulation.

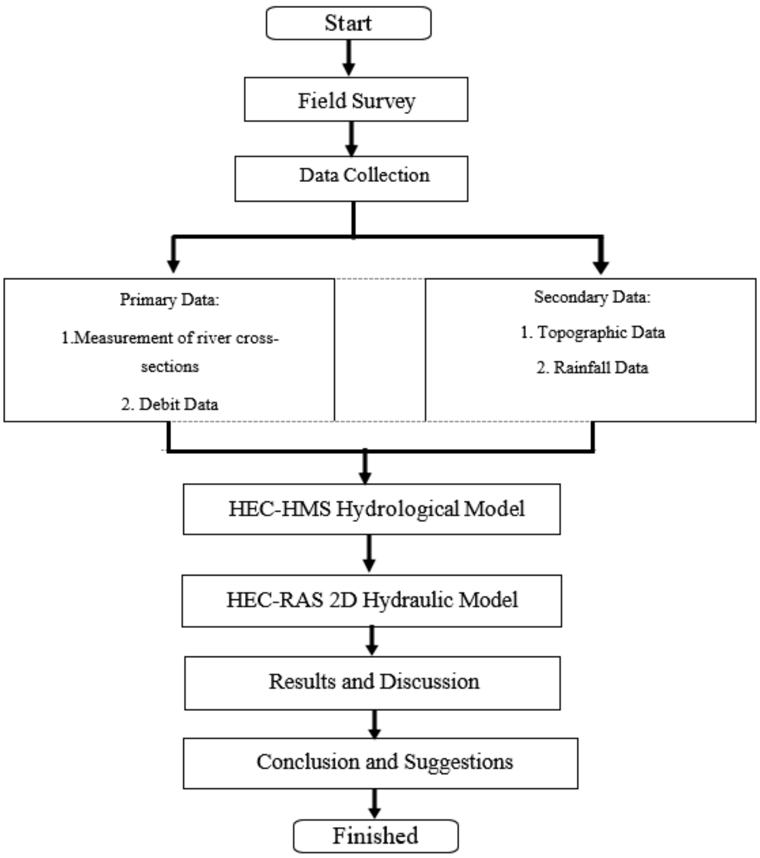

Figure 2. Integrated workflow linking field data, HEC-HMS rainfall-runoff modeling, HEC-RAS 2D simulation, and spatial interpretation

Hydraulic Modeling and Exposure Classification

The 2017 HEC-HMS discharge hydrograph was used as the upstream inflow boundary for unsteady HEC-RAS 2D modeling. Field-surveyed cross-sectional geometry and terrain information were used to represent the river corridor and surrounding floodplain. The final GIS flood map displays a Transverse Mercator/UTM Zone 51N reference with WGS 1984. The supplied record, however, does not provide a verifiable DEM source and cell size for the computational terrain, the two-dimensional mesh-cell dimensions and refinement rules, breakline specifications, spatial Manning n values, the downstream-boundary formulation, computational time step, or numerical mass-balance diagnostics. Because these factors can influence flood depth and extent (Horritt et al., 2006; Liu et al., 2019; Willis et al., 2019), their absence is reported explicitly in the uncertainty section and summarized later in Table 6.

Village-scale classification is based only on the percentage of the administrative village area mapped as inundated. To make the original low/moderate/high labels transparent, the study-specific thresholds are defined as Low exposure <1.0%, Moderate exposure 1.0% to <2.0%, and High exposure >=2.0%. These thresholds are descriptive categories for this dataset; they are not universal flood-risk standards. Because the analysis does not incorporate exposed population, building value, infrastructure criticality, social vulnerability, coping capacity, or velocity, the resulting class is termed inundation exposure rather than flood risk (Apel et al., 2009; Koks et al., 2015; Li et al., 2019).

RESULTS AND DISCUSSION

Rainfall Data Quality and Areal Rainfall

The completeness check materially changes three annual watershed rainfall values. When both gauges were available, the Ranowangko and Tondano-Paleloan weights were 0.92375 and 0.07625, respectively. For 2015, 2021, and 2024, only the Ranowangko observation is present in the supplied record, so the corrected areal values become 112.40, 135.50, and 109.00 mm rather than 103.83, 125.17, and 100.69 mm. This correction prevents missing observations from depressing the annual-maxima series and responds directly to the statistical-data issue identified during review.

Table 2. Corrected Areal Annual-Maximum Rainfall

Year	Ranowangko (mm)	Tondano (mm)	Areal rainfall (mm)	Missing-data treatment
2014	196.5	110.5	189.94	Both stations
2015	112.4	-	112.40	Available station renormalized
2016	102.0	115.5	103.03	Both stations
2017	92.0	160.2	97.20	Both stations
2018	105.5	126.5	107.10	Both stations
2019	68.5	157.3	75.27	Both stations
2020	107.0	157.3	110.84	Both stations
2021	135.5	-	135.50	Available station renormalized
2022	124.0	99.8	122.15	Both stations
2023	124.0	118.4	123.57	Both stations
2024	109.0	-	109.00	Available station renormalized

The corrected series ranges from 75.27 mm in 2019 to 189.94 mm in 2014 and has a mean of 116.91 mm. Figure 3 shows the Thiessen-polygon representation used to define gauge influence. The relatively small Tondano-Paleloan weight means the three corrections are moderate rather than extreme, but their inclusion remains important because annual-maximum frequency analysis is sensitive to systematic bias even when the affected years are not the overall maximum.

Figure 3. Thiessen polygons used to define station influence areas within the Nuay watershed.

Frequency Analysis and Design Rainfall

Descriptive statistics for the corrected annual-maxima sample indicate positive skewness, consistent with a right-tailed extreme-rainfall series. The raw-series skewness is 1.601 and the Pearson kurtosis is 7.327. After base-10 logarithmic transformation, the skewness decreases to 0.635. This provides a reasonable empirical basis for retaining the LP3 family for this small sample, while recognizing that distribution selection from only 11 annual maxima is uncertain. An approximate one-sample Kolmogorov-Smirnov diagnostic on the fitted log-space Pearson Type III distribution gives D = 0.176 and p approximately 0.828. Because distribution parameters were estimated from the same short sample, the p-value should be interpreted as an indicative fit check rather than as a fully independent test.

Table 3. Statistical Summary of the Corrected Annual-Maximum Series

Statistic	Value
Number of annual maxima	11
Mean rainfall	116.91 mm
Sample standard deviation	28.78 mm
Coefficient of variation	0.246
Raw skewness	1.601
Pearson kurtosis	7.327
Mean log10 rainfall	2.0572
SD log10 rainfall	0.0987
Log-space skewness	0.635
Approx. LP3 KS statistic D	0.176
Approx. p-value	0.828

The revised LP3 quantiles increase monotonically with return period, from 111.39 mm at 2 years to 283.57 mm at 1,000 years. Compared with the earlier table, the revised upper-tail values are higher because both the missing-data correction and direct refitting to the corrected series alter the log-space distribution parameters. Table 4 reports these rainfall quantiles transparently. They should not be interpreted as newly simulated design discharges: the HEC-HMS project file required to rerun each return period is not available in the supplied revision package. Reporting rainfall quantiles while withholding unsupported discharge values is preferable to inferring discharge through an unvalidated proportional relationship.

Table 4. Revised Log Pearson Type III Design Rainfall

Return period (years)	Design rainfall (mm)
2	111.39
5	136.71
10	154.35
25	177.65
50	195.77
100	214.56
200	234.17
1000	283.57

Values are frequency-analysis rainfall quantiles based on the corrected 2014-2024 areal annual-maxima series; they are not simulated peak discharges.

The design-rainfall results are consistent with the broader principle that uncertainty increases toward rare return periods, particularly when the record is short. Flood-hazard mapping studies at regional and global scales also emphasize that extreme-event estimates should be interpreted in relation to observation density and model structure (Alfieri et al., 2014; Dottori et al., 2016; Sampson et al., 2015). For the Nuay catchment, the 100- to 1,000-year rainfall estimates are useful for scenario awareness but should not be treated as precise design standards without a longer record or regional frequency analysis.

2017 HEC-HMS Event Reconstruction

The supplied HEC-HMS event summary provides the most directly traceable discharge result in the study. For the 19 February 2017 simulation, the model reports a peak discharge of 20.0 m3/s at 03:00, with precipitation volume of 77.34 mm, loss volume of 48.42 mm, excess rainfall volume of 28.92 mm, direct runoff volume of 28.92 mm, baseflow volume of 23.80 mm, and total discharge volume of 52.72 mm. These quantities are reported in Table 5 so that the central hydrological result is not confined to a screenshot. The parameter summary and event hydrograph indicate a rapid rise shortly after rainfall, consistent with the behavior expected in a relatively small catchment with a one-hour lag parameter.

Table 5. Traceable HEC-HMS Results and Retained Event Parameters for 19 February 2017

Variable	Value
Peak discharge	20.0 m3/s
Time of peak	03:00, 19 Feb 2017
Precipitation volume	77.34 mm
Loss volume	48.42 mm
Excess rainfall volume	28.92 mm
Direct runoff volume	28.92 mm

Variable	Value
Baseflow volume	23.80 mm
Discharge volume	52.72 mm
Curve Number	64
Recession constant	0.4
Ratio to peak	0.6
Initial discharge	0.142813 m3/s
Lag time	60 min

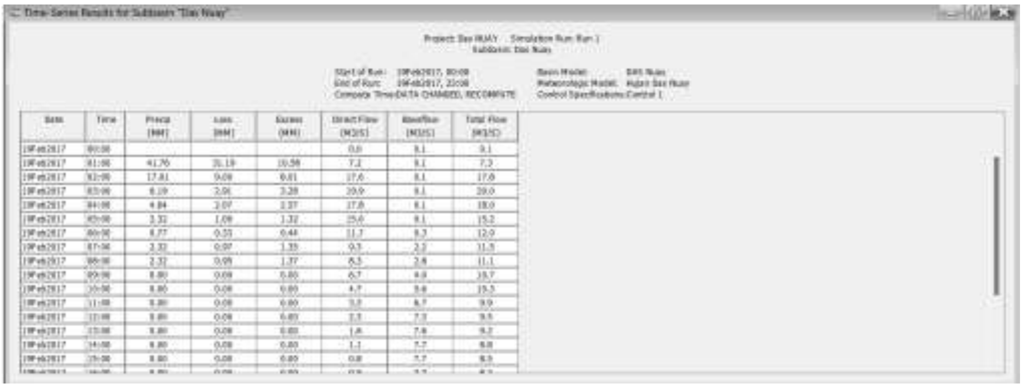

Figure 4. Hydrological computation output retained in the event-reconstruction record.

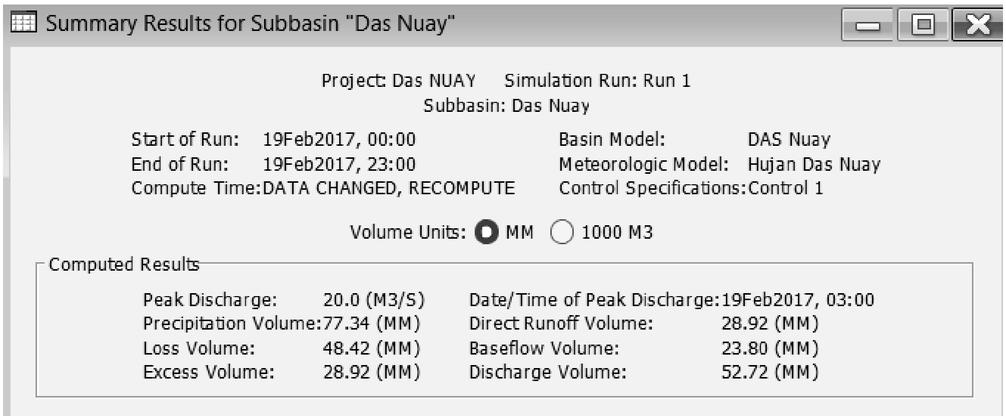

Figure 5. HEC-HMS event summary for 19 February 2017, including the 20.0 m3/s peak discharge.

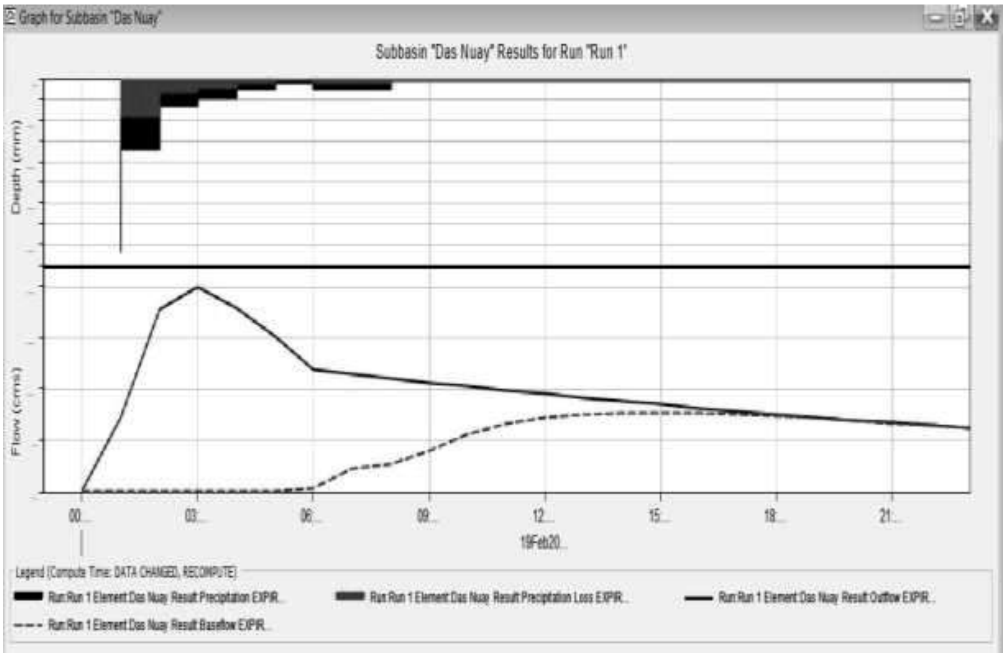

Figure 6. Simulated 2017 Nuay subbasin hydrograph showing a rapid rise and recession response.

The rapid modeled response is hydrologically plausible but should not be overinterpreted as a validated causal diagnosis. The source manuscript associates rapid response with watershed morphology, land use, and limited infiltration. These mechanisms are physically reasonable and are consistent with the coupled-model literature, yet this study did not conduct counterfactual land-use simulations or independent infiltration experiments. The results therefore support an interpretation that catchment size, topographic connectivity, infiltration representation through CN, and channel conveyance jointly shape the event response, rather than establishing the isolated causal effect of any single land-use factor. Similar caution is recommended in data-scarce coupled models, where equifinality among parameters can reproduce comparable hydrographs (Li et al., 2019; Mkhonta et al., 2026).

Hydraulic Response and Flood Inundation

The HEC-RAS analysis translates the hydrological inflow into water-surface and inundation behavior along the Nuay corridor. Figures 7-9 show the upstream, middle, and downstream cross-sectional profiles used to represent the surveyed river geometry, while Figure 10 documents field measurement activity. The sections vary markedly in width and bank form. In the modeled event, relatively narrow and low-capacity portions of the river provide plausible locations for flow to exceed channel conveyance, particularly where adjacent terrain is low. This interaction between hydrograph magnitude, channel geometry, and floodplain elevation is a standard control on two-dimensional inundation patterns (Horritt & Bates, 2002; Hunter et al., 2007; Teng et al., 2017).

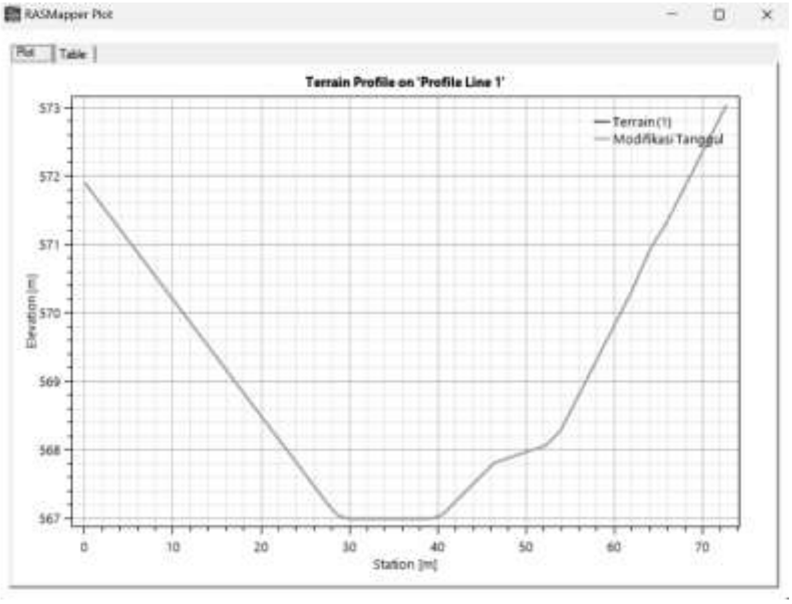

Figure 7. Upstream cross-sectional geometry used to represent the Nuay River channel.

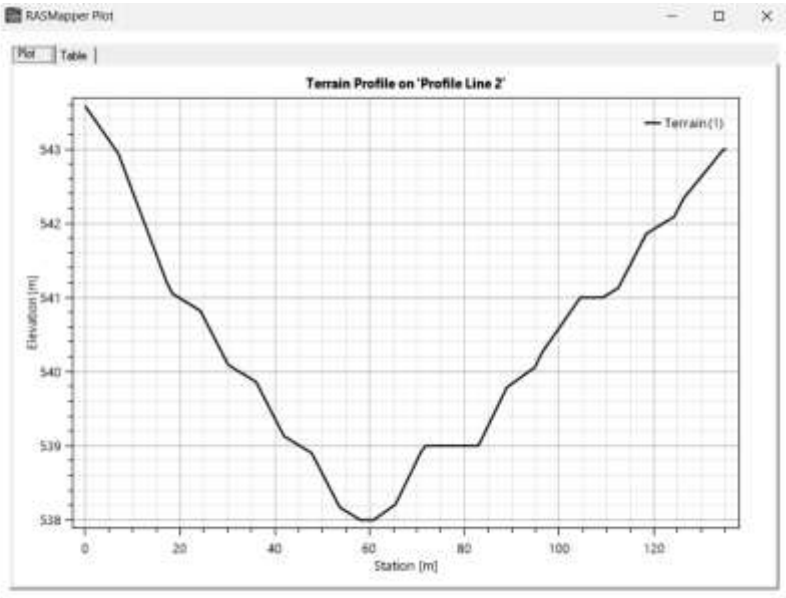

Figure 8. Middle cross-sectional geometry used to represent the Nuay River channel.

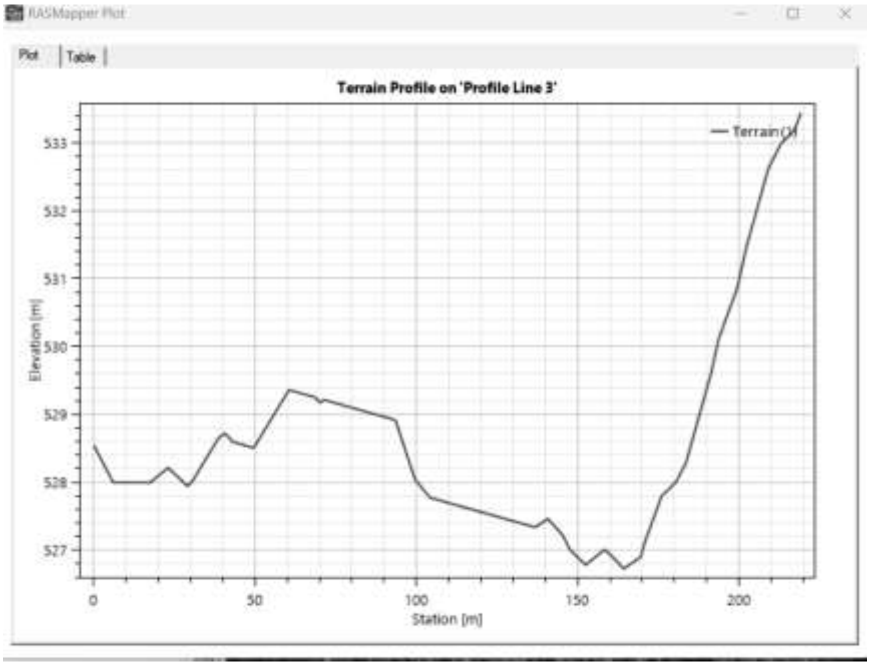

Figure 9. Downstream cross-sectional geometry showing the wider surveyed floodplain profile.

Figure 10. Field measurement of existing Nuay River geometry used as hydraulic-model input.

Figure 11 shows the boundary-condition interface retained in the project record. The 2017 inflow hydrograph was imposed at the upstream side, but the supplied material does not provide enough information to reconstruct the downstream condition or numerical-control settings. Table 6 therefore separates known hydraulic documentation from missing metadata. This is important because two-dimensional flood models can be sensitive to mesh size, terrain smoothing, roughness assignment, time step, and boundary treatment. Comparative HEC-RAS and LISFLOOD-FP studies demonstrate that model structure and grid or terrain configuration can materially affect local depth and inundation extent (Shustikova et al., 2019; Liu et al., 2019), while uncertainty studies identify hydrological inflow and friction among key sources of output variability (Willis et al., 2019).

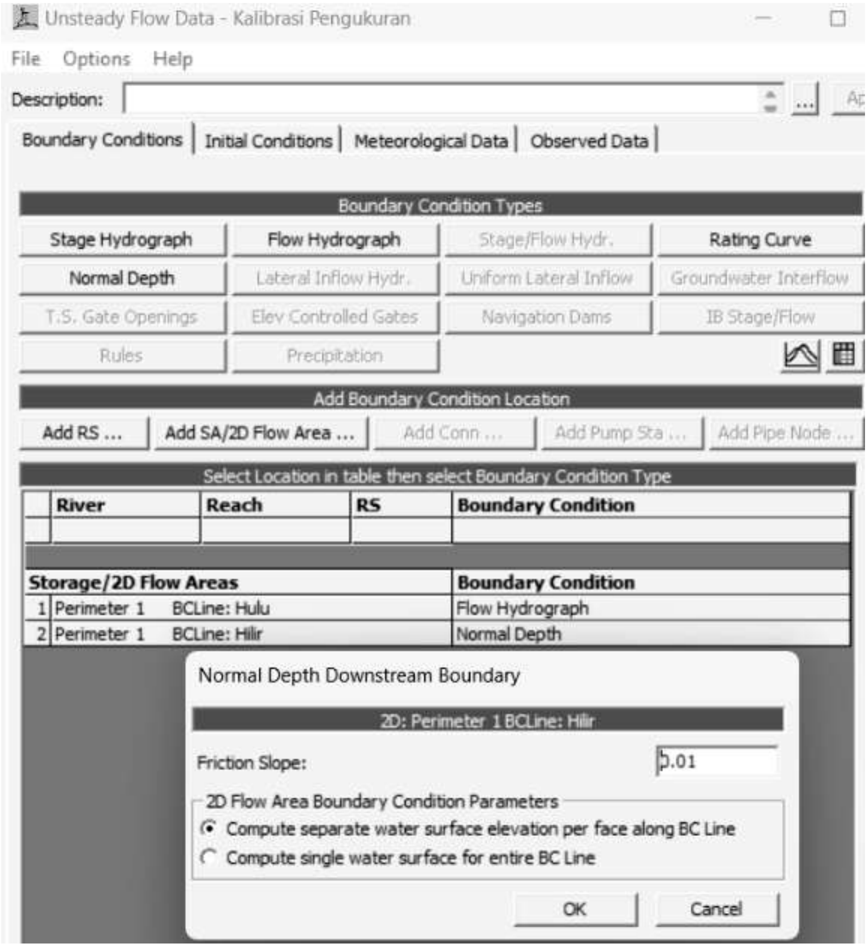

Figure 11. HEC-RAS reach-boundary condition interface retained in the original project record.

Table 6. Hydraulic-Model Documentation and Reproducibility Status

Model element	Information available	Status
Hydraulic formulation	HEC-RAS 2D, unsteady flow	Documented
Upstream condition	2017 HEC-HMS discharge hydrograph	Documented
Channel geometry	Field-surveyed cross sections	Documented
Map coordinate reference	UTM Zone 51N, WGS 1984	Visible in final map metadata
Displayed depth classes	<1, 1, 2, 3, 4, and 5 m	Visible in final map legend
Velocity output	Not reported	Unavailable for exposure classification
HEC-RAS software version	Not verifiable in supplied record	Reproducibility limitation
Terrain/DEM source and resolution	Not verifiable in supplied record	Reproducibility limitation

Model element	Information available	Status
2D mesh size/refinement/breaklines	Not verifiable in supplied record	Reproducibility limitation
Manning's n spatial assignment	Not verifiable in supplied record	Reproducibility limitation
Downstream boundary condition	Not verifiable in supplied record	Reproducibility limitation
Computational time step/duration	Not verifiable in supplied record	Reproducibility limitation
Mass-balance/stability diagnostics	Not reported	Reproducibility limitation

The two-dimensional simulation shown in Figure 12 places inundated cells along the river corridor, and the GIS products in Figures 13 and 14 show that flooding is concentrated in low-lying areas adjacent to the channel. This spatial pattern is physically consistent with the local topographic control expected in floodplain routing. Similar studies show that two-dimensional models are particularly useful for visualizing lateral propagation and flow pathways that are difficult to communicate from channel water levels alone (Bates et al., 2010; Luo et al., 2022). Recent flash-flood applications further demonstrate the value of connecting post-event evidence, channel constrictions, and mapped depth to identify locations where conveyance limitations intensify local hazard (Xu et al., 2025).

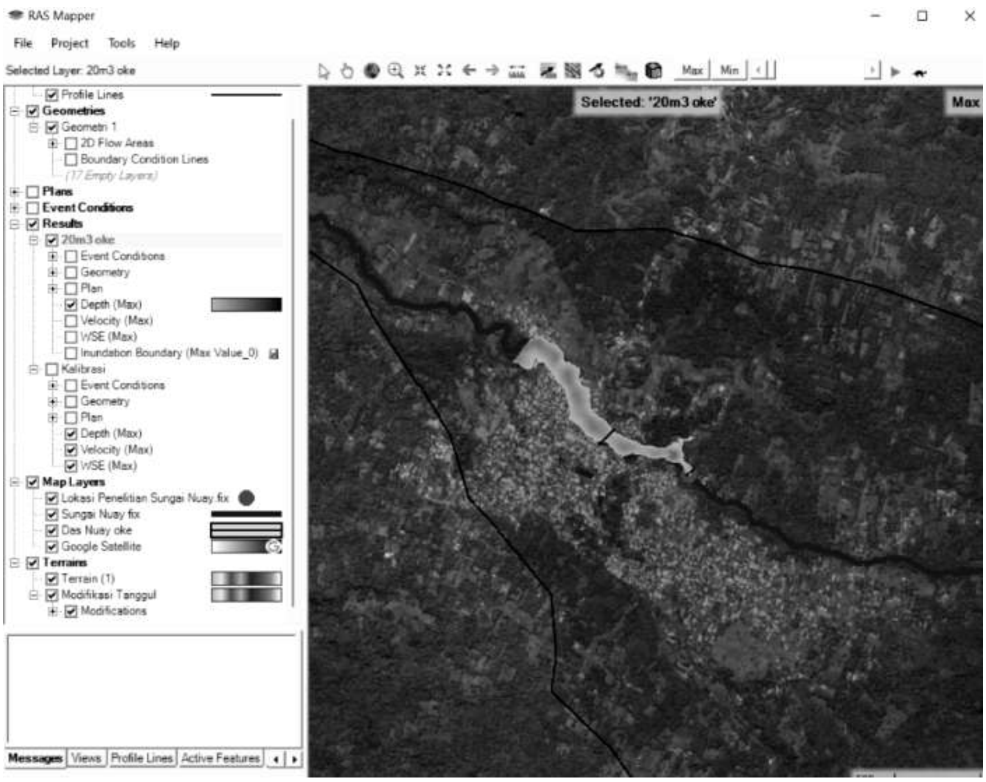

Figure 12. HEC-RAS 2D simulation view showing the modeled 2017 inundation corridor.

Figure 13. GIS flood mapping for the 2017 event across the Nuay watershed and surrounding administrative areas.

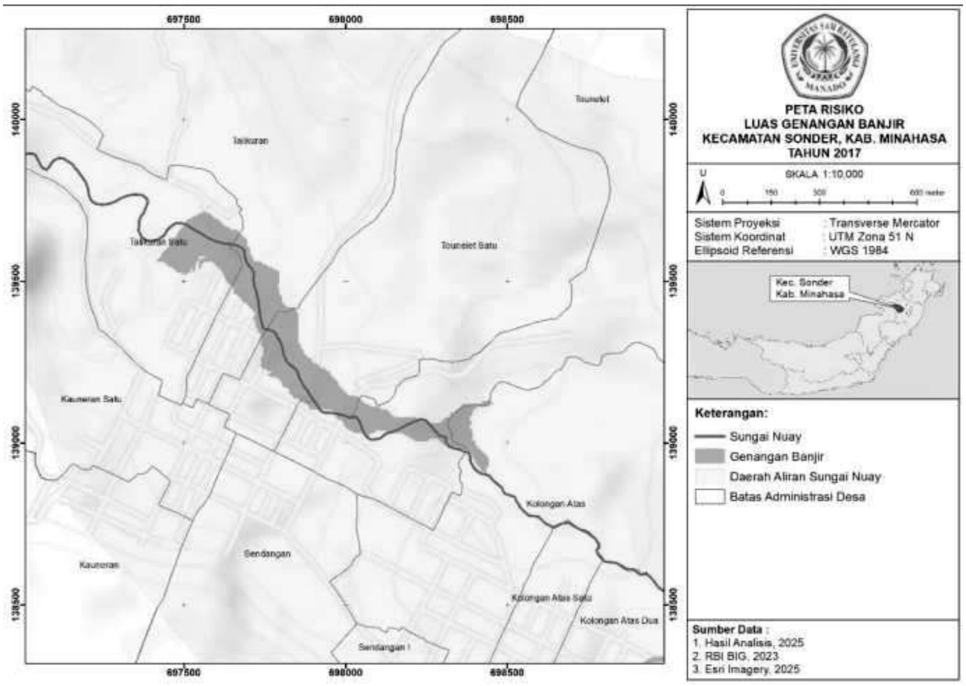

Figure 14. GIS map of the 2017 modeled flood-inundation area along the Nuay River.

Village-Scale Inundation Exposure

The area-based results show clear spatial differentiation among the five villages intersected by the mapped inundation footprint. Talikuran Satu has the largest inundated proportion, 3.2% of its 99.38 ha administrative area, followed by Tounelet Satu with 2.1% of 202.42 ha. Talikuran and Tounelet fall in the study-specific Moderate exposure class at 1.4% and 1.3%, while Kolongan Atas is Low at 0.9%. The absolute flooded area is greatest in Tounelet Satu at 4.30 ha. Because the ranking is based on inundated-area percentage, a small village can receive a higher exposure class even when its absolute flooded area is smaller than that of a larger village. Both metrics should therefore be considered when prioritizing interventions.

Table 7. Village-Scale Inundation Exposure during the Reconstructed 2017 Flood

No.	Village	Flooded area (ha)	Administrative area (ha)	Inundated area (%)	Exposure class
1	Kolongan Atas	1.08	115.11	0.9%	Low
2	Tounelet	2.44	195.30	1.3%	Moderate
3	Talikuran	2.56	186.88	1.4%	Moderate
4	Tounelet Satu	4.30	202.42	2.1%	High
5	Talikuran Satu	3.19	99.38	3.2%	High

Study-specific descriptive thresholds: Low <1.0%; Moderate 1.0% to <2.0%; High >=2.0%. The classification is an inundation-exposure proxy and does not represent comprehensive flood risk.

Figure 15 displays the modeled flood-depth classes along the river. The legend provides classes from less than 1 m through 5 m; however, the supplied record does not provide cell-level summary statistics from which a verified maximum, mean depth, or velocity distribution can be calculated. The map is therefore used to identify the spatial pattern of depth classes rather than to report a fabricated single maximum. Depth and especially depth-velocity combinations would strengthen future hazard classification because they are more directly related to hydraulic intensity than inundated area alone (Mudashiru et al., 2021; Jeong et al., 2024).

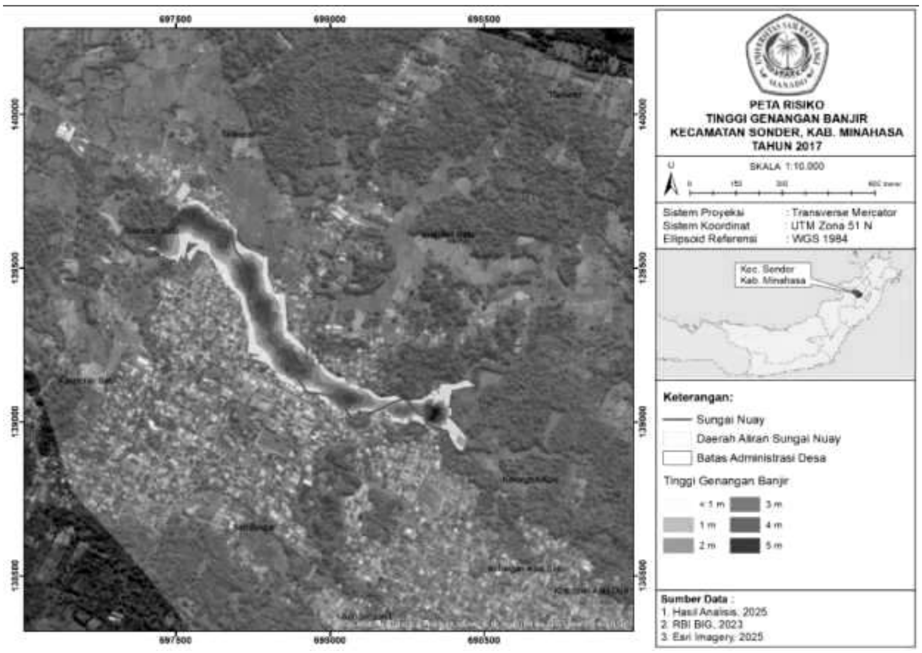

Figure 15. HEC-RAS 2D flood-depth map for the 2017 Nuay River event; the displayed legend contains depth classes from <1 m to 5 m.

Scientific Interpretation and Mitigation Implications

The combined results support a process interpretation in which a rapid catchment hydrograph interacts with spatially variable channel conveyance and adjacent low terrain to produce localized overbank inundation. This interpretation is stronger than a purely descriptive map because the HEC-HMS output provides the temporal inflow forcing and the field-based cross sections provide a physical basis for hydraulic routing. At the same time, it remains a screening-level reconstruction rather than a fully validated predictive system. Studies that benchmark two-dimensional models with high-resolution LiDAR or independent inundation observations show how strongly evaluation quality improves when the model can be checked against observed water levels or flood outlines (Fewtrell et al., 2011; Wing et al., 2017). Future Nuay work should therefore prioritize independent event observations, permanent gauge data, high-water marks, and repeatable terrain datasets.

For mitigation, the spatial concentration of exposure suggests that Tounelet Satu and Talikuran Satu merit priority field verification and detailed engineering assessment. Appropriate actions may include maintaining or restoring channel conveyance at constricted segments, protecting riparian corridors, reducing obstruction at bridges or culverts where verified, conserving infiltration-supporting land cover in the contributing catchment, and incorporating mapped inundation zones into settlement and emergency-route planning. These recommendations should be screened against field surveys before structural intervention because hydraulic modification can transfer hazard downstream. Risk-informed planning should also add population, building, agricultural, and critical-infrastructure exposure so that physical hazard is connected to consequences, as recommended in multidimensional flood-risk frameworks (Merz et al., 2010; Koks et al., 2015).

At the planning scale, the study demonstrates the practical value of coupling models even when observations are limited. Large-scale hazard frameworks show that physically based flood mapping can guide prioritization across data-sparse areas, but local decision making benefits from higher-resolution data and site-specific verification (Sampson et al., 2015; Wing et al., 2017). The Nuay application thus occupies an intermediate role: it provides spatial evidence that is more informative than a discharge-only assessment, while its uncertainty is too large for unqualified use as a final engineering-design or insurance-risk product. This distinction is central to responsible transfer of the findings.

Uncertainty, Limitations, and Transferability

Five limitations define the confidence envelope of the present results. First, the rainfall-frequency analysis uses only 11 annual maxima, so upper-tail return-period estimates have large sampling uncertainty. Second, three station observations are missing; the revised analysis corrects the earlier zero-weighting problem by renormalizing to the available station, but it cannot reconstruct the unobserved spatial rainfall field. Third, the 2017 hydrological calibration evidence is based on community-reported stage information without a preserved continuous discharge hydrograph or rating relationship. Formal NSE, KGE, RMSE, and PBIAS statistics and independent validation are therefore unavailable. Fourth, several key HEC-RAS setup details are missing from the project record, including terrain resolution, mesh configuration, spatial roughness, downstream boundary condition, computational time step, and mass-balance diagnostics. Fifth, the exposure classification uses inundated-area percentage and does not include population, assets, social vulnerability, velocity, or depth-integrated hazard metrics.

These limitations do not invalidate the observed spatial pattern, but they constrain its use. Hydraulic-model literature shows that terrain and roughness uncertainty can shift inundation boundaries and local depths even where the overall pattern remains stable (Horritt et al., 2006; Liu et al., 2019; Willis et al., 2019). Likewise, flash-flood sensitivity studies in ungauged basins demonstrate that hydrological parameters can propagate nonlinearly into risk estimates (Li et al., 2019). The most robust conclusions here are therefore the corrected rainfall statistics, the traceable 2017 HEC-HMS peak reported in the supplied model output, the relative concentration of mapped inundation along low-lying river-adjacent areas, and the village ordering derived from mapped inundated-area percentages.

Transferability to other small tropical catchments should focus on the workflow rather than on the numerical thresholds. The method of documenting missing rainfall, separating event reconstruction from design scenarios, coupling hydrology to two-dimensional hydraulics, and distinguishing hazard or exposure from risk is broadly transferable. In contrast, the CN, lag time, inundation percentages, and

Low/Moderate/High thresholds are site- and event-specific. Recent reviews of deterministic hydrologic-hydraulic coupling similarly emphasize that transfer to data-scarce basins is possible only when local constraints, calibration evidence, and uncertainty are documented explicitly (Mkhonta et al., 2026).

CONCLUSION

The revised integrated analysis shows that the Nuay watershed has a rapid modeled response during the reconstructed 19 February 2017 event and that coupling HEC-HMS with HEC-RAS 2D provides a spatially interpretable representation of flood inundation. Correcting the handling of missing Tondano-Paleloan observations changes the 2015, 2021, and 2024 areal annual maxima to 112.40, 135.50, and 109.00 mm, respectively; the refitted Log Pearson Type III distribution yields design rainfall ranging from 111.39 mm for the 2-year return period to 283.57 mm for the 1,000-year return period. The traceable 2017 HEC-HMS output reports a 20.0 m3/s peak at 03:00. Mapped inundation is concentrated near the river and low-lying terrain, with the highest village-area proportions in Talikuran Satu (3.2%) and Tounelet Satu (2.1%). These percentages are appropriately interpreted as inundation exposure, not comprehensive flood risk, because the study does not include population, asset, vulnerability, or velocity components. The outputs can support prioritization of field verification, channel and riparian management, emergency planning, and more detailed flood-risk assessment, but engineering decisions should account for the short rainfall record, non-gauged event calibration evidence, absence of an independent validation event, and incomplete hydraulic-model metadata.

Data And Model Availability

Rainfall values, summary hydrological parameters, field-geometry figures, GIS maps, and model-output images used in this revision are contained in the supplied manuscript package. The rainfall source is identified in the manuscript as the Sulawesi River Basin Organization I. The complete HEC-HMS and HEC-RAS project directories, raw DEM/terrain layer, detailed mesh and roughness files, rating-curve or paired discharge-observation series, and cell-level hydraulic output tables were not included in the supplied materials and therefore cannot be redistributed or independently reconstructed from this revision. Reproducibility would be improved by archiving those project files and metadata in an institutional repository, subject to data-provider restrictions.

Acknowledgment

The authors express their gratitude to Universitas Sam Ratulangi for institutional support, to the Institute for Research and Community Service (LPPM) for facilitating research activities, and to the local communities, field survey teams, and related parties who contributed to data collection, field observations, and technical discussions. Appreciation is also extended to the agencies that provided hydrometeorological and spatial information used in the study.

REFERENCES

Alfieri, L., Salamon, P., Bianchi, A., Neal, J., Bates, P., & Feyen, L. (2014). Advances in pan-European flood hazard mapping. Hydrological Processes, 28(13), 4067-4077. https://doi.org/10.1002/hyp.9947

Apel, H., Aronica, G. T., Kreibich, H., & Thieken, A. H. (2009). Flood risk analyses-how detailed do we need to be? Natural Hazards, 49(1), 79-98. https://doi.org/10.1007/s11069-008-9277-8

Bates, P. D., Horritt, M. S., & Fewtrell, T. J. (2010). A simple inertial formulation of the shallow water equations for efficient two-dimensional flood inundation modelling. Journal of Hydrology, 387(1-2), 33-45. https://doi.org/10.1016/j.jhydrol.2010.03.027

de Moel, H., van Alphen, J., & Aerts, J. C. J. H. (2009). Flood maps in Europe-methods, availability and use. Natural Hazards and Earth System Sciences, 9, 289-301. https://doi.org/10.5194/nhess-9-289-2009

Dottori, F., Salamon, P., Bianchi, A., Alfieri, L., Hirpa, F. A., & Feyen, L. (2016). Development and evaluation of a framework for global flood hazard mapping. Advances in Water Resources, 94, 87-102. https://doi.org/10.1016/j.advwatres.2016.05.002

El-Bagoury, H., & Gad, A. (2024). Integrated hydrological modeling for watershed analysis, flood prediction, and mitigation using meteorological and morphometric data, SCS-CN, HEC-HMS/RAS, and QGIS. Water, 16(2), 356. https://doi.org/10.3390/w16020356

Fewtrell, T. J., Duncan, A., Sampson, C. C., Neal, J. C., & Bates, P. D. (2011). Benchmarking urban flood models of varying complexity and scale using high resolution terrestrial LiDAR data. Physics and Chemistry of the Earth, Parts A/B/C, 36(7-8), 281-291. https://doi.org/10.1016/j.pce.2010.12.011

Gupta, H. V., Kling, H., Yilmaz, K. K., & Martinez, G. F. (2009). Decomposition of the mean squared error and NSE performance criteria: Implications for improving hydrological modelling. Journal of Hydrology, 377(1-2), 80-91. https://doi.org/10.1016/j.jhydrol.2009.08.003

Horritt, M. S., & Bates, P. D. (2002). Evaluation of 1-D and 2-D numerical models for predicting river flood inundation. Journal of Hydrology, 268(1-4), 87-99. https://doi.org/10.1016/S0022-1694(02)00121-X

Horritt, M. S., Bates, P. D., & Mattinson, M. J. (2006). Effects of mesh resolution and topographic representation in 2-D finite volume models of shallow water fluvial flow. Journal of Hydrology, 329(1-2), 306-314. https://doi.org/10.1016/j.jhydrol.2006.02.016

Hunter, N. M., Bates, P. D., Horritt, M. S., & Wilson, M. D. (2007). Simple spatially-distributed models for predicting flood inundation: A review. Geomorphology, 90(3-4), 208-225. https://doi.org/10.1016/j.geomorph.2006.10.021

Jeong, C., Chegal, S.-D., Kim, D.-H., & Lee, S.-O. (2024). Comparison of FLUMEN and HEC-RAS 2D models for flash flood inundation in urban landscape. Proceedings of Engineering and Technology Innovation, 28, 55-66. https://doi.org/10.46604/peti.2024.13794

Koks, E. E., Jongman, B., Husby, T. G., & Botzen, W. J. W. (2015). Combining hazard, exposure and social vulnerability to provide lessons for flood risk management. Environmental Science & Policy, 47, 42-52. https://doi.org/10.1016/j.envsci.2014.10.013

Li, W., Lin, K., Zhao, T., Lan, T., Chen, X., Du, H., & Chen, H. (2019). Risk assessment and sensitivity analysis of flash floods in ungauged basins using coupled hydrologic and hydrodynamic models. Journal of Hydrology, 572, 108-120. https://doi.org/10.1016/j.jhydrol.2019.03.002

Liu, Z., Merwade, V., & Jafarzadegan, K. (2019). Investigating the role of model structure and surface roughness in generating flood inundation extents using one- and two-dimensional hydraulic models. Journal of Flood Risk Management, 12(1), e12347. https://doi.org/10.1111/jfr3.12347

Luo, P., Luo, M., Li, F., Qi, X., Huo, A., Wang, Z., He, B., Takara, K., Nover, D., & Wang, Y. (2022). Urban flood numerical simulation: Research, methods and future perspectives. Environmental Modelling & Software, 156, 105478. https://doi.org/10.1016/j.envsoft.2022.105478

Merz, B., Kreibich, H., Schwarze, R., & Thieken, A. (2010). Assessment of economic flood damage. Natural Hazards and Earth System Sciences, 10, 1697-1724. https://doi.org/10.5194/nhess-10-1697-2010

Mkhonta, G., Byaruhanga, N., & Kibirige, D. (2026). Towards improved flood prediction: A review of deterministic hydrologic-hydraulic model coupling. Natural Hazards, 122, Article 342. https://doi.org/10.1007/s11069-026-07992-3

Montolalu, T. M., Mananoma, T., & Tangkudung, H. (2021). Tinjauan kapasitas penampang terhadap banjir rencana di Sungai Karis Kecamatan Sonder Kabupaten Minahasa. Jurnal Sipil Statik, 9(1), 65-74.

Moriasi, D. N., Arnold, J. G., Van Liew, M. W., Bingner, R. L., Harmel, R. D., & Veith, T. L. (2007). Model evaluation guidelines for systematic quantification of accuracy in watershed simulations. Transactions of the ASABE, 50(3), 885-900. https://doi.org/10.13031/2013.23153

Mudashiru, R. B., Sabtu, N., Abustan, I., & Balogun, W. (2021). Flood hazard mapping methods: A review. Journal of Hydrology, 603, 126846. https://doi.org/10.1016/j.jhydrol.2021.126846

Nash, J. E., & Sutcliffe, J. V. (1970). River flow forecasting through conceptual models part I-A discussion of principles. Journal of Hydrology, 10(3), 282-290. https://doi.org/10.1016/0022-1694(70)90255-6

Neal, J., Schumann, G., & Bates, P. (2012). A subgrid channel model for simulating river hydraulics and floodplain inundation over large and data sparse areas. Water Resources Research, 48(11), W11506. https://doi.org/10.1029/2012WR012514

Peker, I. B., Gulbaz, S., Demir, V., Orhan, O., & Beden, N. (2024). Integration of HEC-RAS and HEC-HMS with GIS in flood modeling and flood hazard mapping. Sustainability, 16(3), 1226. https://doi.org/10.3390/su16031226

Salem, H. P., Sumarauw, J. S. F., & Wuisan, E. M. (2016). Pola distribusi hujan jam-jaman di Kota Manado dan sekitarnya. Jurnal Sipil Statik, 4(3), 203-210.

Sampson, C. C., Smith, A. M., Bates, P. D., Neal, J. C., Alfieri, L., & Freer, J. E. (2015). A high-resolution global flood hazard model. Water Resources Research, 51(9), 7358-7381. https://doi.org/10.1002/2015WR016954

Shustikova, I., Domeneghetti, A., Neal, J. C., Bates, P., & Castellarin, A. (2019). Comparing 2D capabilities of HEC-RAS and LISFLOOD-FP on complex topography. Hydrological Sciences Journal, 64(14), 1769-1782. https://doi.org/10.1080/02626667.2019.1671982

Teng, J., Jakeman, A. J., Vaze, J., Croke, B. F. W., Dutta, D., & Kim, S. (2017). Flood inundation modelling: A review of methods, recent advances and uncertainty analysis. Environmental Modelling & Software, 90, 201-216. https://doi.org/10.1016/j.envsoft.2017.01.006

Willis, T., Wright, N., & Sleigh, A. (2019). Systematic analysis of uncertainty in 2D flood inundation models. Environmental Modelling & Software, 122, 104520. https://doi.org/10.1016/j.envsoft.2019.104520

Wing, O. E. J., Bates, P. D., Sampson, C. C., Smith, A. M., Johnson, K. A., & Erickson, T. A. (2017). Validation of a 30 m resolution flood hazard model of the conterminous United States. Water Resources Research, 53(9), 7968-7986. https://doi.org/10.1002/2017WR020917

Wilar, W. T., Sumarauw, J. S. F., & Supit, C. J. (2024). Analisis neraca air Sungai Nuay di titik Bendung Nuay Desa Tounelet Kecamatan Sonder Kabupaten Minahasa. TEKNO, 22(88), 809-819. https://doi.org/10.35793/jts.v22i88.55393

Xu, Z., Wang, X., & He, B. (2025). Hydrological and hydraulic modelling of flash flood induced by extreme rainfall in Liulin town, Hubei province, China, 2021. Engineering Applications of Computational Fluid Mechanics, 19(1), 2562107. https://doi.org/10.1080/19942060.2025.2562107